$W^{\pm}H^{\mp}$ associated production at the CERN Large Hadron Collider

A. A. Barrientos Bendezú and B. A. Kniehl

Max-Planck-Institut für Physik (Werner-Heisenberg-Institut), Föhringer Ring 6, 80805 Munich, Germany
(Received 23 July 1998; published 1 December 1998)

We study the production of a charged Higgs boson in association with a W boson at the CERN Large Hadron Collider in the context of the minimal supersymmetric extension of the standard model. This production mechanism is particularly promising if the charged Higgs boson is too heavy to be generated by top-quark decay. We compare the contributions due to $b\bar{b}$ annihilation at the tree level and gg fusion, which proceeds at one loop. Apart from the total cross section, we also consider distributions in transverse momentum and rapidity. We also assess the viability of $W^{\pm}H^{\mp}$ associated production at the Fermilab Tevatron after the installation of the Main Injector and the Recycler. [S0556-2821(98)06123-2]

I. INTRODUCTION

Despite the successful confirmation of the standard model (SM) of elementary particle physics by experimental precision tests during the past few years, the structure of the Higgs sector has essentially remained unexplored, and there is still plenty of room for extensions. A phenomenologically interesting extension of the SM Higgs sector that keeps the electroweak ρ parameter [1] at unity in the Born approximation is obtained by adding a second complex isospin-doublet scalar field with opposite hypercharge. This leads to the two-Higgs-doublet model (2HDM). After the three massless Goldstone bosons which emerge via the electroweak symmetry breaking are absorbed to become the longitudinal degrees of freedom of the $W^{\pm}$ and Z bosons, there remain five physical Higgs scalars: the neutral CP-even h^0 and H^0 bosons, the neutral CP-odd A^0 boson, and the charged $H^{\pm}$-boson pair. In order to avoid flavor-changing neutral currents, one usually assumes that all up-type fermions couple to one of the Higgs doublets while all down-type fermions couple to the other one (2HDM of type II). The Higgs sector of the minimal supersymmetric extension of the SM (MSSM) consists of such a 2HDM of type II. At the tree level, the MSSM Higgs sector has two free parameters, which are usually taken to be the mass m_{A^0} of the A^0 boson and the ratio $\tan\beta = v_2/v_1$ of the vacuum expectation values of the two Higgs doublets.

The search for Higgs bosons and the study of their properties are among the prime objectives of the Large Hadron Collider (LHC), a proton-proton colliding-beam facility with a center-of-mass (c.m.) energy $\sqrt{S} = 14$ GeV presently under construction at CERN [2]. At the LHC, the integrated luminosity is expected to reach $L = 100$ fb^{-1} per year and experiment. In this connection, most of the attention has been focused on the neutral Higgs bosons, and even corrections from quantum chromodynamics (QCD) to their production cross sections and decay widths have been computed [3]. Here, we wish to discuss the prospects of detecting $H^{\pm}$ bosons at the LHC. For $H^{\pm}$-boson masses $m_H < m_t - m_b$, the dominant production mechanisms are $gg, q\bar{q} \to t\bar{t}$ followed by $t \to bH^+$ and/or the charge-conjugate decay [2]. The dominant decay modes of $H^{\pm}$ boson in this mass range are $H^+ \to \bar{\tau}\nu_\tau$ and $H^- \to \tau\bar{\nu}_\tau$ unless $\tan\beta < \sqrt{m_c/m_\tau} \approx 1$ [2]. In

contrast to the SM top-quark events, this signature violates lepton universality, a criterion which is routinely applied in ongoing $H^{\pm}$-boson searches at the Fermilab $p\bar{p}$ collider Tevatron [4]. For larger values of m_H, the most copious sources of $H^{\pm}$ bosons are provided by $gb \to tH^-$ [5,6], $gg \to t\bar{b}H^-$ [7], $qb \to q'bH^+$ [8], and the charge-conjugate subprocesses. The preferred decay channels are then $H^+ \to t\bar{b}$ and $H^- \to \bar{t}b$, independently of $\tan\beta$ [2]. Unfortunately, these signal processes are bound to be obscured by large QCD backgrounds due to $gb \to t\bar{t}b$, $g\bar{b} \to t\bar{t}\bar{b}$, and $gg \to t\bar{t}b\bar{b}$, or by misidentification backgrounds due to $gg, q\bar{q} \to gt\bar{t}$ and $gq \to t\bar{t}q$ [6]. H^+H^- pair production, which proceeds at the tree level via the Drell-Yan process $q\bar{q} \to H^+H^-$, where a photon and a Z-boson are exchanged in the s channel [9],[1] and at one loop via gg fusion $gg \to H^+H^-$ [10], is also severely plagued by such QCD backgrounds.

An attractive way out is to produce the $H^{\pm}$ bosons in association with $W^{\mp}$ bosons, so that the leptonic decays of the latter may serve as a spectacular trigger for the $H^{\pm}$-boson search. The dominant subprocesses of $W^{\pm}H^{\mp}$ associated production are $b\bar{b} \to W^{\pm}H^{\mp}$ at the tree level and $gg \to W^{\pm}H^{\mp}$ at one loop. They were numerically evaluated under LHC conditions in Ref. [11], for $m_b = 0$. In this approximation, the $\bar{b}bh^0$, $\bar{b}bH^0$, and $\bar{b}bA^0$ couplings, which are large for $\tan\beta \gg 1$, are nullified, and the $\bar{b}tH^-$ coupling is wrongly suppressed for $\tan\beta \gg 1$. Thus, the analysis of Ref. [11] is only valid for $\tan\beta \approx 1$. In fact, the authors of Ref. [11] only selected values from the interval $0.3 \le \tan\beta \le 2.3$. Furthermore, the values for m_t and $\sqrt{S}$ and the parton density functions (PDF's) adopted in Ref. [11] are now obsolete. The purpose of this paper is to generalize the analysis of Ref. [11] for arbitrary values of $\tan\beta$ and to update it. Furthermore, we shall include the leading radiative corrections to the relations between the relevant MSSM parameters [12], which were not yet available at the time when Ref. [11] appeared.

---

[1]In the case $q = b$, there are additional Feynman diagrams involving the top quark in the t channel and the h^0 and H^0 bosons in the s channel.

In contrast to Ref. [11], which concentrated on the total cross section, we shall also investigate distributions in transverse momentum p_T and rapidity y. Finally, we shall also consider $W^\pm H^\mp$ associated production at the Tevatron after the completion of the Main Injector and the Recycler (Run II). One expects the integrated luminosity per year and experiment then to be as high as $L = 2$ fb^{-1}, so that this process might provide an interesting alternative, for moderate values of m_H, besides the usual $H^\pm$-production mechanism via top-quark decay.

The literature also contains a discussion of $gg \to W^\pm H^\mp t\bar{t}$ [13]. However, since the top quark turned out to be so heavy, this process is less interesting due to the substantial phase-space suppression relative to $gg, b\bar{b} \to W^\pm H^\mp$.

As for $b\bar{b}$ annihilation, it should be noted that the treatment of bottom as an active flavor inside the colliding hadrons leads to an effective description, which comprises contributions from the higher-order subprocesses $gb \to W^\pm H^\mp b$, $g\bar{b} \to W^\pm H^\mp \bar{b}$, and $gg \to W^\pm H^\mp b\bar{b}$. If all these subprocesses are to be explicitly included along with $b\bar{b} \to W^\pm H^\mp$, then it is necessary to employ a judiciously subtracted bottom PDF in order to avoid double counting [5,13,14]. The evaluation of $b\bar{b} \to W^\pm H^\mp$ with an unsubtracted bottom PDF is expected to slightly overestimate the true cross section [5,13,14]. For simplicity, we shall nevertheless adopt this effective approach in our analysis, keeping in mind that a QCD-correction factor below unity is to be applied.

This paper is organized as follows. In Sec. II, we shall present some analytic results for the cross section of $W^\pm H^\mp$ associated hadroproduction via $b\bar{b}$ annihilation and gg fusion in the 2HDM and outline our calculation of the box amplitude. In Sec. III, we shall quantitatively analyze the size of this cross section and estimate the number of expected signal events at the LHC and the upgraded Tevatron. Section IV contains our conclusions.

II. DETAILS OF THE CALCULATION

We start by defining the kinematics of the inclusive reaction $AB \to WH + X$, where A and B are colliding hadrons, which are taken to be massless. Let $\sqrt{S}$ be the energy of the initial state and y and p_T the rapidity and transverse momentum of the W boson in the c.m. system of the collision. By four-momentum conservation, $m_T \cosh y \leq (S + m_W^2 - m_H^2)/(2\sqrt{S})$, where $m_T = \sqrt{m_W^2 + p_T^2}$ is the transverse mass of the W boson. The hadron A is characterized by its PDF's $F_{a/A}(x_a, M_a)$, where x_a is the fraction of the four-momentum of A which is carried by the (massless) parton a ($p_a = x_a p_A$), M_a is the factorization scale, and similarly for B. The Mandelstam variables $s = (p_a + p_b)^2$, $t = (p_a - p_W)^2$, and $u = (p_b - p_W)^2$ at the parton level are thus related to S, y, and p_T by $s = x_a x_b S$, $t = m_W^2 - x_a \sqrt{S} m_T \exp(-y)$, and $u = m_W^2 - x_b \sqrt{S} m_T \exp(y)$, respectively. Notice that $s p_T^2 = tu - m_W^2 m_H^2$. In the parton model, the differential cross section of $AB \to WH + X$ is given by

$$\frac{d^2\sigma}{dy\,dp_T^2}(AB \to WH + X)$$

$$= \sum_{a,b} \int dx_a dx_b F_{a/A}(x_a, M_a) F_{b/B}(x_b, M_b)$$

$$\times s \frac{d\sigma}{dt}(ab \to WH)$$

$$\times \delta(s + t + u - m_W^2 - m_H^2)$$

$$= \sum_{a,b} \int_{\bar{x}_a}^1 dx_a F_{a/A}(x_a, M_a) F_{b/B}(x_b, M_b)$$

$$\times \frac{x_b s}{m_H^2 - t} \frac{d\sigma}{dt}(ab \to WH), \tag{2.1}$$

where $\bar{x}_a = [\sqrt{S} m_T \exp(y) - m_W^2 + m_H^2]/[S - \sqrt{S} m_T \exp(-y)]$ and $x_b = [x_a \sqrt{S} m_T \exp(-y) - m_W^2 + m_H^2]/[x_a S - \sqrt{S} m_T \exp(y)]$ in the last expression. The parton-level cross section is calculated from the $ab \to WH$ transition-matrix element $\mathcal{T}$ as $d\sigma/dt = \overline{|\mathcal{T}|^2}/(16\pi s^2)$, where the average is over the spin and color degrees of freedom of the partons a and b.

We now turn to the specific subprocesses $ab \to WH$. For generality, we work in the 2HDM, adopting the Feynman rules from Ref. [15]. For definiteness, however, we shall concentrate on the MSSM in the numerical analysis in Sec. III. We neglect the Yukawa couplings of the first- and second-generation quarks. For later use, we define here the propagator functions

$$\mathcal{S}_t(s) = \frac{1}{\sin\beta}\left(\frac{\cos\alpha\,\cos(\alpha-\beta)}{s - m_{h^0}^2 + i m_{h^0}\Gamma_{h^0}} + \frac{\sin\alpha\,\sin(\alpha-\beta)}{s - m_{H^0}^2 + i m_{H^0}\Gamma_{H^0}}\right),$$

$$\mathcal{S}_b(s) = \frac{1}{\cos\beta}\left(\frac{-\sin\alpha\,\cos(\alpha-\beta)}{s - m_{h^0}^2 + i m_{h^0}\Gamma_{h^0}}\right.$$

$$\left. + \frac{\cos\alpha\,\sin(\alpha-\beta)}{s - m_{H^0}^2 + i m_{H^0}\Gamma_{H^0}}\right),$$

$$\mathcal{P}_t(s) = \frac{\cot\beta}{s - m_{A^0}^2 + i m_{A^0}\Gamma_{A^0}},$$

$$\mathcal{P}_b(s) = \frac{\tan\beta}{s - m_{A^0}^2 + i m_{A^0}\Gamma_{A^0}}. \tag{2.2}$$

Here, α is the mixing angle that rotates the weak CP-even Higgs eigenstates into the mass eigenstates h^0 and H^0, m_{h^0} and Γ_{h^0} are the pole mass and total decay width of the h^0 boson, respectively, and similarly for the H^0 and A^0 bosons.

At the tree level, $W^\pm H^\mp$ associated production proceeds via $b\bar{b}$ annihilation. Here, we treat the b and $\bar{b}$ quarks as active partons inside the colliding hadrons A and B. This should be a useful picture at such high energies, $\sqrt{S} > m_W + m_H$. For consistency with the underlying infinite-momentum frame, we neglect the bottom-quark mass. However, we must not suppress terms proportional to m_b in the
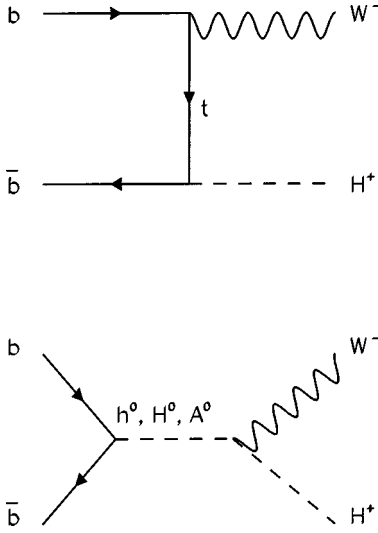
FIG. 1. Feynman diagrams for $b\bar{b}\rightarrow W^- H^+$.

FIG. 2. Typical Feynman diagrams for $gg\rightarrow W^- H^+$.

Yukawa couplings, since they generally dominate the related m_t-dependent terms if $\tan\beta$ is large enough, typically for $\tan\beta\gtrsim\sqrt{m_t/m_b}\approx 6$. This is obvious for the $\bar{b}tH^-$ vertex, which has the Feynman rule [15]

$$i2^{-1/4}G_F^{1/2}[m_t\cot\beta(1+\gamma_5)+m_b\tan\beta(1-\gamma_5)],$$
$$(2.3)$$

where G_F is Fermi's constant and we have neglected the Cabibbo-Kobayashi-Maskawa mixing, i.e., $V_{tb}=1$. The relevant Feynman diagrams are depicted in Fig. 1. The diagrams involving the h^0, H^0, or A^0 bosons are suppressed if $\tan\beta$ is of order unity, but they are indispensable if $\tan\beta\gtrsim\sqrt{m_t/m_b}$. They were neglected, along with the terms proportional to m_b in Eq. (2.3), in Ref. [11], where the restricted range $0.3\leqslant\tan\beta\leqslant 2.3$ was considered. The parton-level cross section of $b\bar{b}\rightarrow W^- H^+$ reads

$$\frac{d\sigma}{dt}(b\bar{b}\rightarrow W^- H^+)$$

$$=\frac{G_F^2}{24\pi s}\left\{\frac{m_b^2}{2}\lambda(s,m_W^2,m_H^2)(|\mathcal{S}_b(s)|^2+|\mathcal{P}_b(s)|^2)\right.$$

$$+\frac{m_b^2\tan\beta}{t-m_t^2}(m_W^2 m_H^2-sp_T^2-t^2)$$

$$\times\text{Re}(\mathcal{S}_b(s)-\mathcal{P}_b(s))$$

$$+\frac{1}{(t-m_t^2)^2}[m_t^4\cot^2\beta(2m_W^2+p_T^2)$$

$$\left.+m_b^2\tan^2\beta(2m_W^2 p_T^2+t^2)]\right\},$$
$$(2.4)$$

where $\lambda(x,y,z)=x^2+y^2+z^2-2(xy+yz+zx)$ is the Källén function. The one of $b\bar{b}\rightarrow W^+ H^-$ emerges through charge conjugation, by substituting $t\leftrightarrow u$ on the right-hand side of Eq. (2.4).

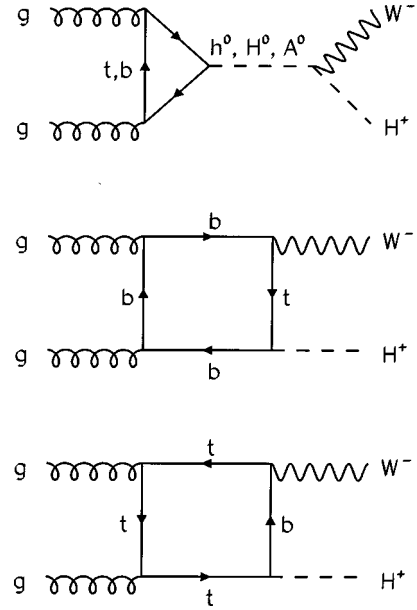An alternative $W^\pm H^\mp$ production mechanism is provided by gluon fusion, which proceeds at one loop via the triangle-type and box diagrams depicted in Fig. 2. In the MSSM, there are additional loop contributions due to squarks, which decouple in the limit of their masses being large. In a typical MSSM scenario, these contributions are expected to be negligibly small. Although the parton-level cross section of gluon fusion is suppressed by two powers of α_s relative to the one of $b\bar{b}$ annihilation, it is expected to yield a comparable contribution at multi-TeV hadron colliders, due to the overwhelming gluon luminosity. On the other hand, the bottom PDF may be considered as being generated from $g\rightarrow b\bar{b}$ splitting via the Altarelli-Parisi evolution and is thus of $\mathcal{O}(\alpha_s)$ relative to the gluon PDF. Therefore, both mechanisms are formally of the same order at the hadron level. As we shall see in Sec. III, these two mechanisms indeed compete with each other numerically. Since bottom does not appear as a parton in gg fusion, we keep m_b finite in this case.

The transition-matrix element of $gg\rightarrow W^- H^+$ corresponding to the sum of the triangle-type diagrams in Fig. 2 is given by

$$\mathcal{T}_\Delta=\frac{\sqrt{2}}{\pi}\alpha_s(\mu)G_F m_W\varepsilon_\lambda^*(p_W)(p_a+p_b)^\lambda$$

$$\times\varepsilon_\mu^c(p_a)\varepsilon_\nu^c(p_b)\left[\left(p_b^\mu p_a^\nu-\frac{s}{2}g^{\mu\nu}\right)\Sigma(s)\right.$$

$$\left.+i\varepsilon^{\mu\nu\rho\sigma}p_{a\rho}p_{b\sigma}\Pi(s)\right],$$
$$(2.5)$$

where $\alpha_s(\mu)$ is the strong coupling constant at renormalization scale μ, $\varepsilon_\mu^c(p_a)$ is the polarization four-vector of gluon a and similarly for gluon b and the W boson, it is summed over the color index $c=1,\ldots,8$, and

$$\Sigma(s)=\sum_{q=t,b}\mathcal{S}_q(s)S\left(\frac{s+i\epsilon}{4m_q^2}\right),$$

$$\Pi(s) = \sum_{q=t,b} \mathcal{P}_q(s) P\left(\frac{s+i\epsilon}{4m_q^2}\right). \tag{2.6}$$

Here, we have introduced the auxiliary functions

$$S(r) = \frac{1}{r}\left[1 - \left(1 - \frac{1}{r}\right)\mathrm{arsinh}^2 \sqrt{-r}\right],$$

$$P(r) = -\frac{1}{r}\,\mathrm{arsinh}^2 \sqrt{-r}. \tag{2.7}$$

By analytic continuation, $\mathrm{arsinh}\sqrt{-r} = -i\,\arcsin\sqrt{r}$ $= \mathrm{arcosh}\sqrt{r} - i\pi/2$, where the first, second, and third expressions are appropriate for $r \leq 0$, $0 < r \leq 1$, and $r > 1$, respectively. Notice that $S(r), P(r) \to 0$ as $r \to \infty$, so that the bottom-quark contribution to Eq. (2.5) is suppressed, except for large $\tan\beta$. For reference, we also list the contribution to the cross section of $gg \to W^- H^+$ that is obtained by squaring Eq. (2.5):

$$\frac{d\sigma_\Delta}{dt} = \frac{\alpha_s^2(\mu) G_F^2}{2048\pi^3} \lambda(s, m_W^2, m_H^2)$$

$$\times (|\Sigma(s)|^2 + |\Pi(s)|^2). \tag{2.8}$$

We generated and evaluated the amplitude $\mathcal{T}_\square$ corresponding to the sum of the box diagrams in Fig. 2 with the aid of the computer packages FEYNARTS [16], FEYNCALC [17], and FF [18]. The analytic expression is somewhat lengthy, and we refrain from listing it here. To gain confidence in these tools [16–18] and our use of them, we checked that they allow us to numerically reproduce the differential cross section of $gg \to ZH$ [19] in the SM to very high precision. Finite-m_b effects $\mathcal{T}_\square$ are indispensable for $\tan\beta \gtrsim \sqrt{m_t/m_b}$, which follows from Eq. (2.3). However, neglecting m_b in the bottom propagator, where it cannot be enhanced by $\tan\beta$, should still be a useful approximation. Nevertheless, we also keep m_b finite there. Due to Bose symmetry, the cross section $d\sigma/dt$ of $gg \to W^- H^+$ is symmetric in t and u. Due to charge-conjugation invariance, it coincides with the one of $gg \to W^+ H^-$.

III. NUMERICAL RESULTS

We are now in a position to explore the phenomenological implications of our results. The SM input parameters for our numerical analysis are $G_F = 1.16639 \times 10^{-5}$ GeV^{-2} [20] and the pole masses $m_W = 80.375$ GeV, $m_Z = 91.1867$ GeV, $m_t = 175.6$ GeV [21], and $m_b = 4.7$ GeV. We adopt the lowest-order set CTEQ4L [22] of proton PDF's. We evaluate $\alpha_s(\mu)$ from the lowest-order formula [20] with $n_f = 5$ quark flavors and asymptotic scale parameter $\Lambda_{\mathrm{QCD}}^{(5)} = 181$ MeV [22]. We identify the renormalization and factorization scales with the $W^\pm H^\mp$ invariant mass, $\mu^2 = M_a^2 = M_b^2 = s$. For our purposes, it is useful to select the MSSM input parameters to be $\tan\beta$ and the pole mass m_H of the $H^\pm$ bosons to be produced. We vary them in the ranges $1 < \tan\beta < 40 \approx m_t/m_b$ and 85 GeV $< m_H < 1$ TeV, respectively. For given

values of $\tan\beta$ and m_H, we determine α and the pole masses m_{h^0}, m_{H^0}, and m_{A^0} of the neutral Higgs bosons from the appropriate MSSM relationships [15] including their leading radiative corrections [12] as implemented in the program package HDECAY [23]. In the case of gg fusion, these corrections only modify $\mathcal{T}_\Delta$, since $\mathcal{T}_\square$ does not depend on α, m_{h^0}, m_{H^0}, and m_{A^0}. Similarly, in the case of $b\bar{b}$ annihilation, only the s-channel diagrams are affected. We sum over the $W^+ H^-$ and $W^- H^+$ final states.

We first consider $pp \to W^\pm H^\mp + X$ at the LHC with $\sqrt{S} = 14$ TeV. In Fig. 3(a), the fully integrated cross sections due to $b\bar{b}$ annihilation and gg fusion are shown as functions of m_H for $\tan\beta = 1.5$, 6, and 30. For a comparison with future experimental data, these two contributions should be added. We observe that $b\bar{b}$ annihilation always dominates. Its contribution modestly exceeds the one due to gg fusion, by a factor of two or less, if $\tan\beta \gtrsim 1$ and $m_H > 200$ GeV, but it is more than one order of magnitude larger if $m_H < m_t$. The gg-fusion contribution is greatly suppressed if $\tan\beta \gtrsim 6$, independently of m_H. For all values of $\tan\beta$, the latter exhibits a dip located about $m_H = m_t$, which arises from resonating top-quark propagators in $\mathcal{T}_\square$. In Fig. 3(b), the $\tan\beta$ dependence of $\sigma(pp \to W^\pm H^\mp + X)$ is displayed for $m_H = 100$, 300, and 1000 GeV. In the case of $m_H = 100$ GeV, the $b\bar{b}$ and gg contributions exhibit minima at $\tan\beta \approx 6$. As m_H increases, these minima migrate to smaller and larger values of $\tan\beta$, respectively. It is interesting to compare $b\bar{b}$ annihilation and gg fusion with regard to their kinematic behavior. This is done for the p_T and y distributions in Figs. 4(a) and 4(b), respectively, assuming $\tan\beta = 1.5$, 6, 30 and $m_H = 300$ GeV. In general, the $b\bar{b}$ and gg cross sections have similar line shapes and just differ in their overall normalizations. In the case of gg fusion, it is instructive to analyze the interplay of $\mathcal{T}_\Delta$ and $\mathcal{T}_\square$. Figure 5 compares the gg-fusion results shown in Fig. 3(b) with the respective contributions proportional to $|\mathcal{T}_\Delta|^2$ [see Eq. (2.8)] and $|\mathcal{T}_\square|^2$. The latter two are comparable in size and up to one order of magnitude larger than the full result. Obviously, there is a strong destructive interference between $\mathcal{T}_\Delta$ and $\mathcal{T}_\square$. For a typical MSSM scenario [23] with $\tan\beta$ and m_H in the ranges considered here, the relative shift in the gg ($b\bar{b}$) cross section due to the MSSM radiative corrections [12] does not exceed the order of 10% (1%) in magnitude.

As advertised in Sec. I, one of the potential phenomenological advantages of $W^\pm H^\mp$ associated production is the circumstance that the charged leptons originating from the decaying $W^\pm$ bosons can be utilized as a clean trigger. Isolated, energetic electrons and muons will be hard to miss, and τ leptons should be identifiable with high efficiency via their one-prong decays to electrons, muons, charged pions, or charged kaons, which have a combined branching fraction of about 85% [20]. Thus, approximately 30% of the $W^\pm H^\mp$ signal events should be more or less straightforwardly detectable in this way. If we assume the integrated luminosity per year to be at its design value of $L = 100$ fb^{-1} for each of the two LHC experiments, ATLAS and CMS, then a cross section of 1 fb translates into about 60 detectable $W^\pm H^\mp$
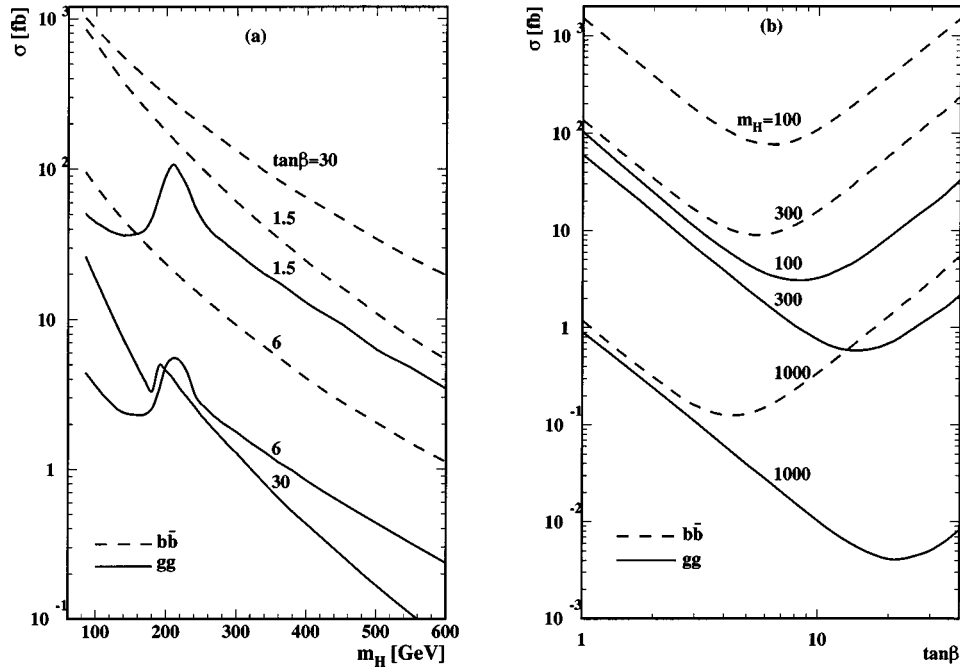
FIG. 3. Total cross sections σ (in fb) of $pp \to W^\pm H^\mp + X$ via $b\bar{b}$ annihilation (dashed lines) and gg fusion (solid lines) at the LHC (a) as functions of m_H for $\tan\beta = 1.5$, 6, and 30; and (b) as functions of $\tan\beta$ for $m_H = 100$, 300, and 1000 GeV.

events per year. Looking at Fig. 3, we thus conclude that, depending on $\tan\beta$, one should be able to collect an annual total of between 650 and 14,000 such events if $m_H = 300$ GeV.

We now turn to $p\bar{p}$ collisions at the Tevatron with $\sqrt{S} = 2$ TeV (Run II). In Fig. 6, the total cross sections due to $b\bar{b}$ annihilation and gg fusion are presented as functions of m_H for $\tan\beta = 1.5$, 6, and 30. During Run II, the Tevatron,

supplemented by the Main Injector and the Recycler, is expected to deliver an integrated luminosity of $L = 2$ fb^{-1} per year to each of the two detectors, CDF and D0. Assuming that the $H^\pm$ bosons can be identified via their decays to τ leptons and that the $W^\pm$ bosons can also be recognized if they decay hadronically, by requiring that the two-jet invariant mass be close to m_W, a cross section of 1 fb hence corresponds to about 20 detectable $W^\pm H^\mp$ events during five
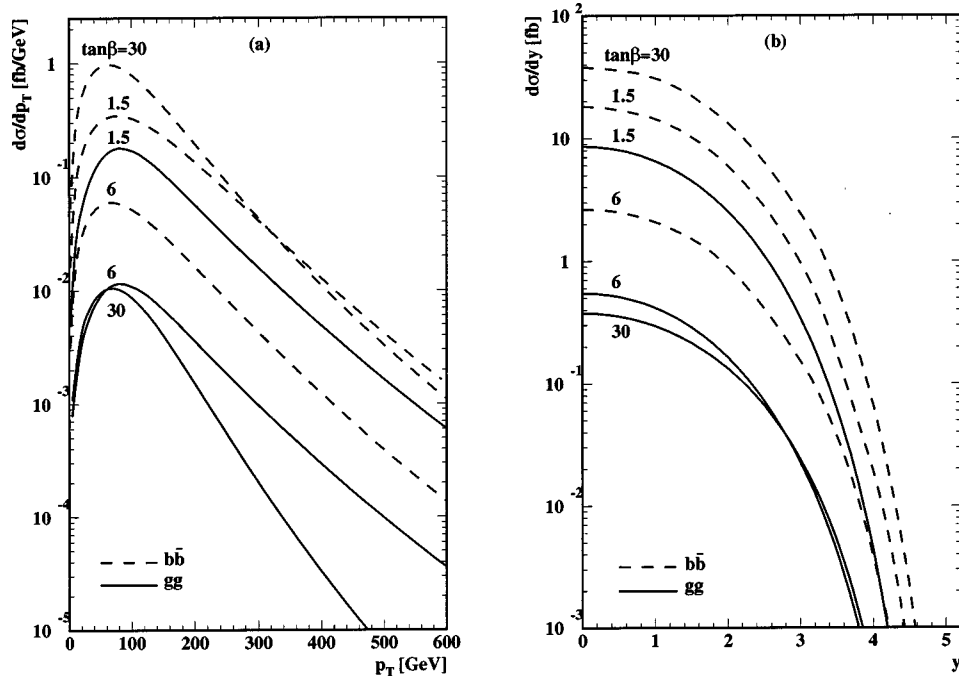

FIG. 4. (a) p_T distributions $d\sigma/dp_T$ (in fb/GeV) and (b) y distributions $d\sigma/dy$ (in fb) of $pp \to W^\pm H^\mp + X$ via $b\bar{b}$ annihilation (dashed lines) and gg fusion (solid lines) at the LHC for $\tan\beta = 1.5$, 6, 30 and $m_H = 300$ GeV.
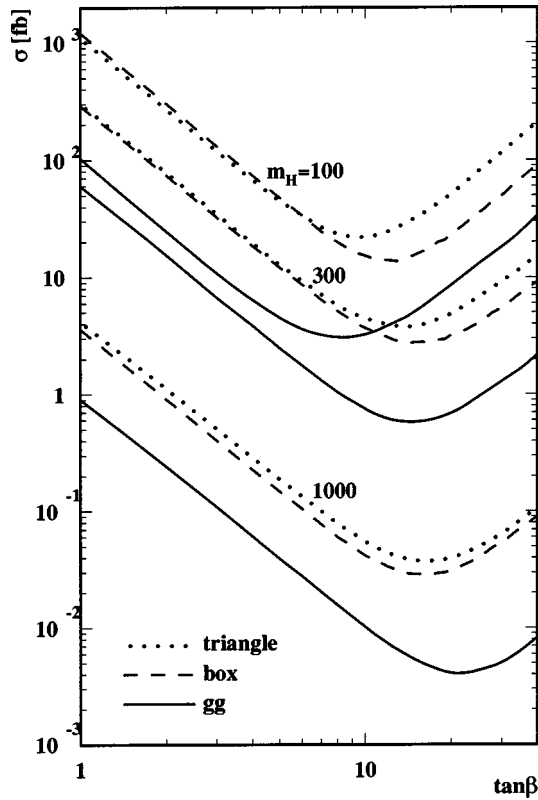
FIG. 5. Total cross section σ (in fb) of $pp \to W^{\pm}H^{\mp}+X$ via gg fusion (solid lines) at the LHC as a function of m_H for $\tan\beta$ = 1.5, 6, and 30. The contributions due to the triangle-type (dotted lines) and box diagrams (dashed lines) are also shown.

FIG. 6. Total cross sections σ (in fb) of $p\bar{p} \to W^{\pm}H^{\mp}+X$ via $b\bar{b}$ annihilation (dashed lines) and gg fusion (solid lines) at the Tevatron (Run II) as functions of m_H for $\tan\beta$=1.5, 6, and 30.

years of operation. From Fig. 6, we read off that, depending on $\tan\beta$, the total yield during that period should range between 5 and 50 if $m_H = 100$ GeV.

Finally, we should compare our analysis with the one reported in Ref. [11]. If we adopt the input information from Ref. [11], we are able to nicely reproduce the results obtained therein, except that our gg-fusion cross section turns out to be a factor of two larger. A possible interpretation of this difference is that, in contrast to the case of $b\bar{b}$ annihilation, the results for gg fusion shown in Figs. 4 and 5 of Ref. [11] actually refer to one of the W^+H^- and W^-H^+ final states rather than to their sum as declared in the text.

IV. CONCLUSIONS

We studied $W^{\pm}H^{\mp}$ associated hadroproduction within the MSSM, allowing for $\tan\beta$ to be arbitrary. We included the contributions from $b\bar{b}$ annihilation and gg fusion to lowest order. For $\tan\beta \gtrsim 6$, the m_b-dependent terms in the relevant Yukawa couplings give rise to significant effects in both channels and must not be neglected. In particular, the s-channel diagrams of Fig. 1 would otherwise be missed. We also incorporated the leading corrections to the relations between the relevant MSSM parameters [12].

Using up-to-date information on the input parameters and proton PDF's, we presented theoretical predictions for the $W^{\pm}H^{\mp}$ production cross section at LHC and Tevatron ener-
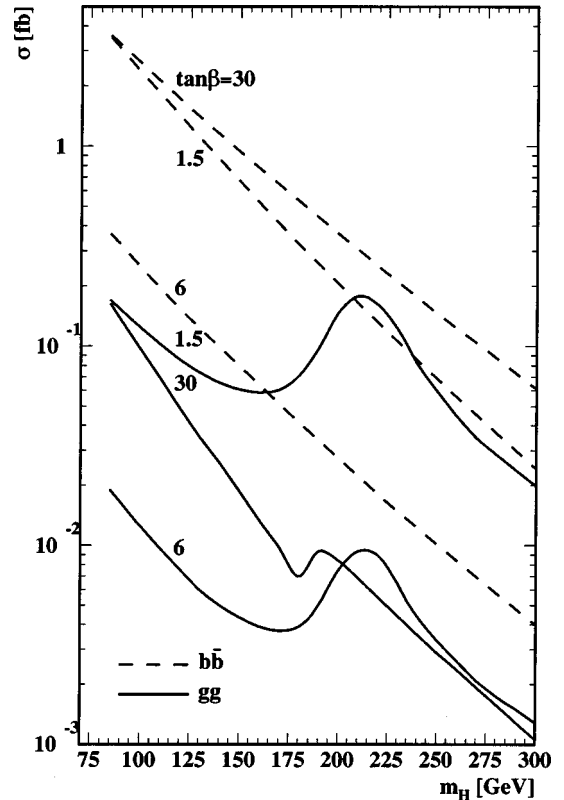
gies. Apart from the fully integrated cross section, we also analyzed distributions in p_T and y. A favorable scenario for $W^{\pm}H^{\mp}$ associated hadroproduction would be characterized by the conditions that $m_H > m_t - m_b$ and that $\tan\beta$ is either close to unity or of order m_t/m_b. Then, the $H^{\pm}$ bosons could not spring from on-shell top quarks, which are so copiously produced at hadron colliders, and their decays to τ leptons, which are relatively easy to identify, would have a small branching fraction. On the other hand, $W^{\pm}H^{\mp}$ production would have a sizeable cross section, and the leptonic $W^{\pm}$ decays would provide a spectacular trigger. We found that the $W^{\pm}H^{\mp}$ signal should have a signicant rate at the LHC unless m_H is very large. The search for this signal could also usefully supplement the standard techniques of looking for $H^{\mp}$ bosons [4] during Run II at the Tevatron.

Note added in proof. After the submission of this manuscript, a paper [24] appeared which reports on a signal-versus-background analysis of $W^{\pm}H^{\mp}$ associated hadroproduction under LHC conditions.

$W^{\pm}H^{\mp}$ ASSOCIATED PRODUCTION AT THE CERN LARGE . . .

PHYSICAL REVIEW D **59** 015009

[1] M. Veltman, Nucl. Phys. **B123**, 89 (1977).

[2] Z. Kunszt and F. Zwirner, Nucl. Phys. **B385**, 3 (1992), and references cited therein.

[3] M. Spira, Fortschr. Phys. **46**, 203 (1998), and references cited therein.

[4] CDF Collaboration, F. Abe *et al.*, Phys. Rev. D **54**, 735 (1996); CDF and D0 Collaborations, B. Bevensee, in proceedings of 33rd Rencontres de Moriond: QCD and High Energy Hadronic Interactions, Les Arcs, France, 1998, Report No. FERMILAB-Conf-98/155-E.

[5] J. F. Gunion, H. E. Haber, F. E. Paige, W.-K. Tung, and S. S. D. Willenbrock, Nucl. Phys. **B294**, 621 (1987); R. M. Barnett, H. E. Haber, and D. E. Soper, *ibid.* **B306**, 697 (1988); F. I. Olness and W.-K. Tung, *ibid.* **B308**, 813 (1988).

[6] V. Barger, R. J. N. Phillips, and D. P. Roy, Phys. Lett. B **324**, 236 (1994).

[7] J. L. Diaz-Cruz and O. A. Sampayo, Phys. Rev. D **50**, 6820 (1994).

[8] S. Moretti and K. Odagiri, Phys. Rev. D **55**, 5627 (1997).

[9] E. Eichten, I. Hinchliffe, K. Lane, and C. Quigg, Rev. Mod. Phys. **56**, 579 (1984); **58**, 1065(E) (1986); N. G. Deshpande, X. Tata, and D. A. Dicus, Phys. Rev. D **29**, 1527 (1984).

[10] S. S. D. Willenbrock, Phys. Rev. D **35**, 173 (1987); J. Yi, M. Wen-Gan, H. Liang, H. Meng, and Y. Zeng-Hui, J. Phys. G **24**, 83 (1998); A. Krause, T. Plehn, M. Spira, and P. M. Zerwas, Nucl. Phys. **B519**, 85 (1998).

[11] D. A. Dicus, J. L. Hewett, C. Kao, and T. G. Rizzo, Phys. Rev. D **40**, 787 (1989).

[12] M. Carena, J. R. Espinosa, M. Quirós, and C. E. M. Wagner, Phys. Lett. B **355**, 209 (1995); M. Carena, M. Quirós, and C. E. M. Wagner, Nucl. Phys. **B461**, 407 (1996); H. E. Haber, R. Hempfling, and A. H. Hoang, Z. Phys. C **75**, 539 (1997).

[13] D. A. Dicus and C. Kao, Phys. Rev. D **41**, 832 (1990).

[14] D. A. Dicus and S. Willenbrock, Phys. Rev. D **39**, 751 (1989).

[15] J. F. Gunion and H. E. Haber, Nucl. Phys. **B272**, 1 (1986); **B278**, 449 (1986); J. F. Gunion, H. E. Haber, G. Kane, and S. Dawson, *The Higgs Hunter's Guide* (Addison-Wesley, Redwood City, CA, 1990).

[16] J. Küblbeck, M. Böhm, and A. Denner, Comput. Phys. Commun. **60**, 165 (1990).

[17] R. Mertig, M. Böhm, and A. Denner, Comput. Phys. Commun. **64**, 345 (1991).

[18] G. J. van Oldenborgh, Comput. Phys. Commun. **66**, 1 (1991).

[19] B. A. Kniehl, Phys. Rev. D **42**, 2253 (1990); **42**, 3100 (1990).

[20] Particle Data Group, C. Caso *et al.*, Eur. Phys. J. C **3**, 1 (1998).

[21] The LEP Collaborations ALEPH, DELPHI, L3, OPAL, the LEP Electroweak Working Group and the SLD Heavy Flavour Group, D. Abbaneo *et al.*, Report No. CERN-PPE/97-154 (1997).

[22] H. L. Lai, J. Huston, S. Kuhlmann, F. Olness, J. Owens, D. Soper, W. K. Tung, and H. Weerts, Phys. Rev. D **55**, 1280 (1997).

[23] M. Spira, Nucl. Instrum. Methods Phys. Res. A **389**, 357 (1997); A. Djouadi, J. Kalinowski, and M. Spira, Comput. Phys. Commun. **108**, 56 (1998).

[24] S. Moretti and K. Oddagiri, Report No. Cavendish-HEP-98/13, RAL-TR-1998-063, and hep-ph/9809244, 1998.